Highly nonlinear excitonic Zeeman spin splitting in composition-engineered artificial atoms

V. Jovanov,[1,*] T. Eissfeller,[1] S. Kapfinger,[1] E. C. Clark,[1] F. Klotz,[1] M. Bichler,[1] J. G. Keizer,[2] P. M. Koenraad,[2] M. S. Brandt,[1] G. Abstreiter,[1] and J. J. Finley[1]

[1]*Walter Schottky Institut and Physik Department, Technische Universität München, Am Coulombwall 4, 85748 Garching, Germany*

[2]*Department of Applied Physics, Eindhoven University of Technology, P.O. Box 513, 5600 MB Eindhoven, The Netherlands*

(Received 12 December 2011; revised manuscript received 14 March 2012; published 16 April 2012)

Nonlinear Zeeman splitting of neutral excitons is observed in composition-engineered $In_xGa_{1-x}As$ self-assembled quantum dots, and its microscopic origin is explained. Eight-band $\mathbf{k}\cdot\mathbf{p}$ simulations, performed using realistic dot parameters extracted from cross-sectional scanning tunneling microscopy measurements, reveal that a quadratic contribution to the Zeeman energy originates from a spin-dependent mixing of heavy- and light-hole orbital states in the dot. The dilute In composition ($x < 0.35$) and large lateral size (40–50 nm) of the quantum dots investigated are shown to strongly enhance the nonlinear contribution to the excitonic Zeeman gap, providing a blueprint to enhance such magnetic nonlinearities via growth engineering of the quantum dots.

DOI: 10.1103/PhysRevB.85.165433 PACS number(s): 78.67.Hc

I. INTRODUCTION

Over the past decade, semiconductor quantum dots (QDs) have attracted significant interest, mainly due to the prospects they provide for integrated, electro-optically addressable quantum systems capable of storing and processing quantum information.[1] Quantum information processing requires the possibility for selective manipulation of a *specific* spin qubit within a quantum register. Such selective addressing using conventionally applied techniques, such as electron spin resonance,[2,3] is rather challenging and can be achieved more conveniently with recently proposed electrical methods for spin control via Landé g-tensor modulation.[4–6] These approaches exploit tuning of the magnetic response by pushing the carrier envelope function into different regions of composition-engineered QD nanostructures. Although electrical g-factor modulation has been successfully demonstrated in composition-graded AlGaAs quantum wells[7] and vertically coupled InGaAs QD molecules[8] for several years, significant tuning of g factors in individual self-assembled dots was achieved only recently.[9,10] It was shown that orbital angular momentum quenching of confined carriers in semiconductor nanostructures[10–12] affects their g factor, which allowed for the control using static electric fields.[10,11] Since most of the experiments addressing the spin of confined carriers are performed in magnetic fields, it is important to develop a microscopic understanding of how *magnetic fields* influence the spin properties of the orbital states.

In this paper, we report strong magnetic-field-induced tuning of the exciton g factor in composition-engineered $In_xGa_{1-x}As$-GaAs self-assembled QDs. By comparing our experimental results with realistic eight-band $\mathbf{k}\cdot\mathbf{p}$ simulations performed using quantum dot size, shape, and compositional information obtained from cross-sectional scanning tunneling microscopy (X-STM), we identify the origins of the magnetic-field dependence of the g factor. Our results show that magnetic fields influence the excitonic g factor via a mechanism that differs fundamentally from the case of static electric fields.[10] In particular, the combination of the rather dilute In composition ($x < 0.35$) and comparatively large lateral size of the dots (40–50 nm) is found to lead to spin-selective mixing of the lowest-energy heavy-hole (HH) and light-hole (LH) orbital states, the strength of which varies with magnetic field. This gives rise to a quadratic $\propto B^2$ contribution to the Zeeman energy gap—a phenomenon previously observed only in semiconductor quantum wells and superlattices.[13,14]

II. SAMPLES AND EXPERIMENTAL TECHNIQUES

Two samples were investigated that consisted electrically tunable GaAs n-i-Schottky photodiode structures into which two different types of QDs were embedded in the i region. Both samples were produced using molecular-beam epitaxy under nominally identical growth conditions. The first sample was grown utilizing the conventional Stranski-Krastanov growth, while in the second the partially covered island (PCI) "In-flushing" method was utilized.[15] In the following, the sample containing the conventionally grown dots is referred to as the *nonflushed* sample, whereas the sample containing the dots grown with the PCI technique is termed *flushed*. Both samples had a single layer of $In_xGa_{1-x}As$ self-assembled QDs grown in the 140-nm-thick i region, using a relatively high growth temperature of 590 °C. The QD layer nominally consisted of 8 ML of $In_xGa_{1-x}As$ with an In content of $x = 0.50$, deposited at a rate of 0.41 ML/s and an As overpressure of 1.5×10^{-5} mbar. The comparatively high growth temperature is expected to lead to an average In content lower than the nominal $x = 0.50$, due to the combined effects of In desorption,[16] interdiffusion with the GaAs matrix material, and In segregation.[17] Comparison of our results with simulations provides strong support for this expectation, showing that the strong tunability of g_{ex} is inextricably linked to a low average $x \approx 0.35$. For the *flushed* sample, a growth interruption was included after the QDs had been partially capped with a 6-nm-thick GaAs layer. During this growth interruption, the temperature was increased to 650 °C and kept constant for 30 s. After this, it was again lowered to the nominal growth temperature and an additional capping layer of GaAs was deposited. A typical topography X-STM image[18] of two representative QDs is presented in the left panel of Fig. 1, revealing that the QDs from the high-density regions of the wafers exhibit inhomogeneous In-composition profiles with a relatively large cross-sectional size of 40–50 nm and a height of 4–8 nm for the *nonflushed* dots and 4–6 nm for

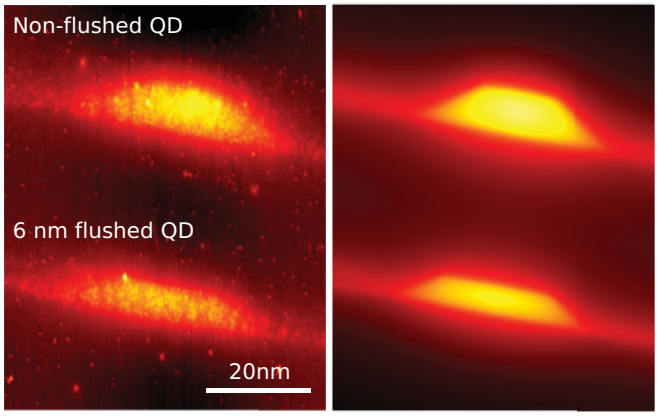

FIG. 1. (Color online) Left panel: Topography X-STM image of a conventionally grown quantum dot and a dot grown using identical conditions but including the In-flush technique. Right panel: Outward relaxation analysis of the two quantum dots from which the absolute In concentration and spatial composition profile in the dots were extracted.

the *flushed* dots. Two different QD composition profiles were successfully fitted to the measured outward relaxation of the cleaved facet: (i) a linearly increasing In concentration from the base to the apex of the dot and (ii) an inverted trumpetlike In distribution.[19–21] The results from the latter are shown in the rightmost panel of Fig. 1. Here, it should be noted that X-STM outward relaxation analysis can yield approximately similar concentration profiles that match the surface topology, and that the method itself does not unambiguously identify which exact composition profile applies to the QDs studied.[22] However, our experimental observations were only found to be in good general accord with theory using the inverted trumpet In-distribution profile. The outward relaxation simulations revealed that for the conventionally grown *nonflushed* QD shown in the left panel of Fig. 1, the In concentration in the apex is $x^{\text{apex}} = 0.35$, reducing to $x^{\text{min}} = 0.22$ near the base of the dot. In contrast, for the *flushed* sample the In concentration at the apex is slightly lower ($x^{\text{apex}} = 0.30$) due to desorption of In during the flush step. These data provide the basis for the dot size, shape, and composition used in the simulations presented below.

Optical characterization of the quantum dots was performed at low temperatures (10 K) using a confocal microscope inserted into a superconducting magnet that provides fields up to 15 T in Faraday configuration.

III. OPTICAL SPECTROSCOPY

Typical photoluminescence (PL) spectra are presented in Fig. 2 from the neutral exciton X^0 of four representative QDs from the *nonflushed* as well as from the *flushed* sample. Many quantum dots (>30) were studied, and the results presented in Fig. 2 illustrate the full range of behaviors that were observed. The polarization-resolved PL spectra from different QDs from the *nonflushed* sample (labeled QD_A, QD_B, and QD_C) and from the *flushed* sample (labeled QD_D) reveal a substantially different behavior of the Zeeman splitting with increasing magnetic field. This can be clearly seen in Fig. 3, where the Zeeman energy, defined as $\Delta E_Z = E(\sigma^+_{\text{det}}) - E(\sigma^-_{\text{det}}) = g_{\text{ex}}\mu_B B$, is plotted for the four dots presented in Fig. 2, as well as for many other dots. Positive, negative, as well as zero excitonic Zeeman splittings were observed for different dots from the same samples.

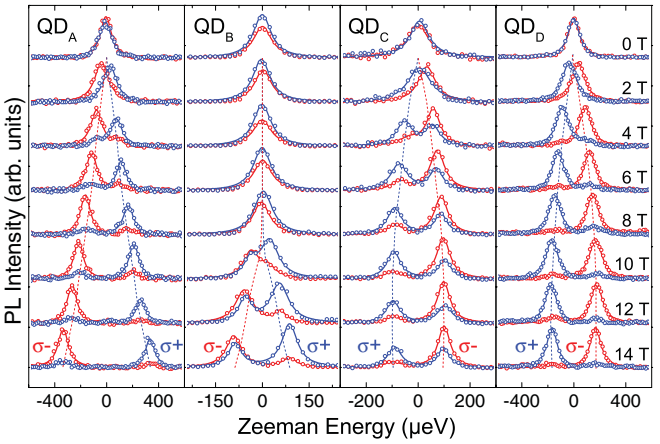

FIG. 2. (Color online) Polarization-resolved photoluminescence spectra of four representative quantum dots grown without (QD_A, QD_B, and QD_C) and with (QD_D) the partially covered island flushing technique.

We show below that the observed variations reflect the range of size and material composition fluctuations measured in our X-STM microscopy studies. A striking feature of the Zeeman splittings presented in Fig. 3 is the nonlinear dependence of ΔE_Z on the magnetic field—a magnetic *field-dependent* exciton g factor: $g_{\text{ex}} = g_e + g_h = g^0_{\text{ex}} + g^1_{\text{ex}} B$. The best fit to the Zeeman splittings of QD_A, QD_B, QD_C, and QD_D was obtained using a quadratic function, as depicted by the solid lines presented in Fig. 3. The solid lines for the other QDs interpolate the experimental data. For all of the QDs investigated, we observed Zeeman splittings for the negatively charged trion X^{-1} that were identical to those of the corresponding neutral excitons X^0. We attribute the pronounced nonlinear dependence of ΔE_Z on B to a strongly magnetic-field-dependent *hole* g factor g_h for QDs

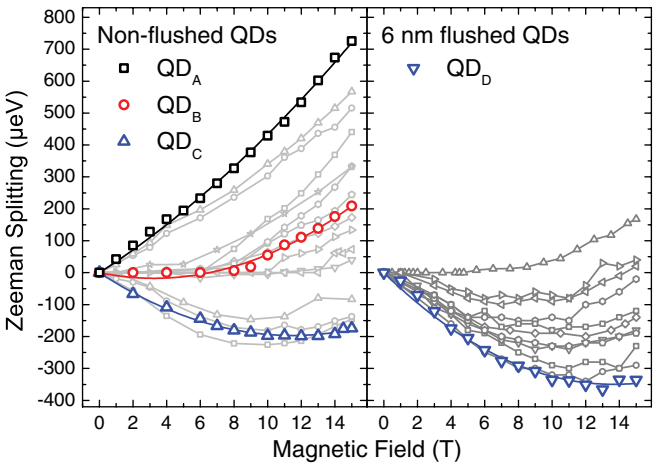

FIG. 3. (Color online) Zeeman splitting of the neutral exciton in several QDs grown without (left) and with the partially covered island flushing technique (right).

with particular lateral size and In-composition profiles, as will be explained in detail below.

While the excitonic Zeeman splittings of the QDs from the *nonflushed* sample revealed positive, negative, and even zero excitonic g factors (Fig. 3, leftmost panel), the dots from the *flushed* sample mainly revealed negative but also B-field-dependent g factors (Fig. 3, rightmost panel). The weaker variation in the Zeeman splittings observed for the dots from the *flushed* sample compared to the *nonflushed* sample arises from the reduced fluctuations in the dot height and the lower average In concentration caused by the PCI growth process.

At this point, we note that the observation of a nonlinear Zeeman splitting is not directly correlated with the degrees of circular polarization DOP $= (I_{\sigma^+} - I_{\sigma^-})/(I_{\sigma^+} + I_{\sigma^-})$ of the emission. This can be clearly seen by comparing the data recorded from QD_C and QD_D presented in Fig. 2. Both of these dots exhibit similar behavior: a negative Zeeman splitting that saturates at higher magnetic fields >10 T. However, despite the similarity in the observed behavior, the two dots exhibit degrees of circular polarization that are both very different from each other and magnetic-field-independent. The dot QD_C exhibits a rather low degree of circular polarization of $37 \pm 1\%$ while QD_D has a DOP of $87 \pm 2\%$, respectively. A large fraction of the dots investigated ($\geqslant$60%) showed the expected circularly polarized eigenstates at elevated magnetic field, regardless of the type of Zeeman splitting they exhibited. However, the low degree of circular polarization for QD_B and QD_C is not in accord with theoretical expectations, and we believe that it arises from the experimental geometry used. For example, since we use Au-dielectric shadow mask apertures with a size close to the optical wavelength in free space ($\approx 1\ \mu$m), the position of the dot under the aperture is highly likely to influence the polarization of the emitted light into the far field.[23] For any situation other than a dot located in the center of the aperture, the reduction of the symmetry of the local dielectric environment may perturb the polarization of the emitted light, leading to the observed complex behavior. Similar effects are well known for the emission of quantum dots in elliptical micropillars[24] or, in an extreme case, the emission from semiconductor nanowires with subwavelength lateral dimensions.[25] Thus, it is difficult to draw quantitative conclusions from the measured degree of circular polarization. In contrast, the Zeeman splitting is a robust experimental quantity and we continue by exploring the microscopic origins of the rich behavior exhibited in Figs. 2 and 3.

IV. DISCUSSION

A weak nonlinear dependence of the electron Zeeman splitting on the magnetic field was first reported for GaAs-AlGaAs quantum wells and superlattices subject to very high magnetic fields.[26] Similar quadratic magnetic-field dependencies of the hole Zeeman splitting have been reported for GaAs-InGaAs superlattices and quantum wells and attributed to a magnetic-field-induced mixing of HH and LH states.[14,27,28] In quantum wells subject to a magnetic field applied parallel to the quantization axis, the hole wave function can be readily factorized in a product of quantum-well states in the vertical direction and Landau levels in the lateral directions.[28,29] A magnetic field applied parallel to the [001] quantization axis induces a coupling between the HH $\uparrow$ subband and the LH $\uparrow$ and LH $\downarrow$ subbands. The strength of this coupling is proportional to $\gamma_3\sqrt{B}\hat{k}_z$ and $(\gamma_2 + \gamma_3)B$ for the LH $\uparrow$ and LH $\downarrow$ subbands, respectively.[30] Here, the operator $\hat{k}_z$ acts in the growth direction, and γ_2 and γ_3 are the Luttinger parameters.[31] Unlike the HH $\uparrow$ subband, the HH $\downarrow$ states couple only to the LH $\uparrow$ subband via an interaction with a strength varying as $(\gamma_2 - \gamma_3)B$. Since $\gamma_2 \approx \gamma_3$ for $In_xGa_{1-x}As$ alloys, the latter coupling is normally negligible[32] and, consequently, the HH $\downarrow$ ground state has an almost pure HH $\downarrow$ character, independent of the magnetic field. It has been shown that the coupling of the HH $\uparrow$ ground state to the light-hole bands leads to a HH g factor that varies linearly with the square of the in-plane wave vector, i.e., $g_h \propto k_\parallel^2$.[28] For quantum-well Landau levels, $k_\parallel^2$ itself varies linearly with magnetic field leading to the experimentally observed quadratic Zeeman splitting. On the other hand, in small, strongly confined quantum dots, $k_\parallel^2$ varies with $\propto 1/D^2$, where D is the dot diameter. As a result, one would expect that the hole g factor in strongly confined dots (i.e., small D) should be unaffected by the magnetic field. These qualitative considerations indicate that the presently studied large QDs with dilute In composition produce effects that fall in a regime between the expectations for quantum wells ($g_h = g_h^0 + g_h^1 B$) and quantum dots (g_h independent of B). We continue by developing these ideas quantitatively to explain our experimental observations.

A. Theoretical model

To understand the microscopic origin of the observed nonlinear Zeeman splitting, we performed three-dimensional electronic-structure calculations using the eight-band $\mathbf{k}\cdot\mathbf{p}$ envelope-function approximation. In order to include the B field, we used the recently proposed gauge-invariant symmetry-adapted finite-element method that accurately accounts for valence-band couplings.[33] Strain fields were included using continuum elasticity theory and their impact on the electronic structure was fully taken into account via deformation potentials and the linear piezoelectric effect.[34] The exchange interaction is expected to be of minor importance for the neutral exciton because of the large effective band gap of $\approx$1320 meV and the weak mixing of conduction- and valence-band states. The direct Coulomb interaction was found to have a negligible influence on the exciton g factor and is, therefore, also neglected in our simulations.[10]

To obtain quantitative results for the X^0 g factor, a Luttinger-like eight-band $\mathbf{k}\cdot\mathbf{p}$ model was employed, where remote-band contributions to the effective-mass Hamiltonian and g factors are included up to the order k^2.[30] We modeled our QDs as having a truncated lens shape with a diameter varying from $D = 25$ to 50 nm, a height of 4 nm above the wetting layer (WL), and an inverse trumpetlike In-compositional profile.[35] The In concentration of the $In_xGa_{1-x}As$ alloy was taken to be $x^{\min} = 0.2$ at the base and side of the dot, increasing to $x^{\text{apex}} = 0.3$–0.5 at the dot apex.[21] These parameters are consistent with the results of X-STM measurements (Fig. 1), from which we also determined the thickness and In content of the wetting layer to be 2 nm and $x^{\text{WL}} = 0.18$, respectively.[18]

The leftmost panel of Fig. 4 shows the calculated exciton Zeeman spin splitting as a function of the magnetic field

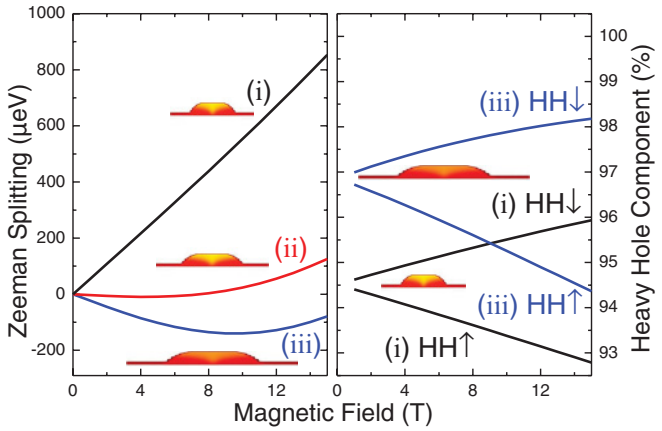

FIG. 4. (Color online) (Left) Calculated Zeeman spin splitting of the neutral exciton in three QDs with the same height of 6 nm but different diameter and In concentration at the apex x^{apex} as a function of the magnetic field: (i) 25 nm diam and $x^{\text{apex}} = 0.50$, (ii) 45 nm diam and $x^{\text{apex}} = 0.45$, (iii) 50 nm diam and $x^{\text{apex}} = 0.40$. (Right) Calculated heavy-hole character of the lowest hole orbital levels having spin-up HH ↑ and spin-down HH ↓ character, respectively.

for three model dots having different size and In composition consistent with the range obtained from our X-STM measurements. These representative QDs have been chosen in order to reproduce the generic behavior of QD_A, QD_B, and QD_C, representing the full range of behaviors observed in our experiments. The In concentration decreases from $x^{\text{apex}} = 0.50$ to 0.40, the data labeled (i) to (iii) in Fig. 4, while the lateral size is increased from 25 nm (i) to 50 nm (iii) in order to reproduce the experimentally observed range of exciton transition energies (1310–1365 meV). The curve labeled (i) in the leftmost panel of Fig. 4 shows an almost purely linear Zeeman splitting (B-field-independent g factor) while (iii) exhibits a clear quadratic dependence. In comparison, the model QD (ii) exhibits a behavior that is intermediate between the linear and quadratic regimes. The quadratic dependence of the exciton Zeeman splitting stems entirely from the HH-like lowest-energy orbital state in the valence band. For all QDs presented in Fig. 4 (i) to (iii), the valence-band Zeeman splitting varies quadratically with magnetic field, namely,

$$\Delta E_Z^h = \mu_B g_h^0 B + \mu_B g_h^1 B^2, \tag{1}$$

where the B field is applied along the growth direction, μ_B is the Bohr magneton, and g_h^0 and g_h^1 are the linear and quadratic components of the hole g factor, respectively.

By fitting a quadratic function to the observed Zeeman splittings in Fig. 3 for QD_A to QD_D, we extracted both the linear $(g_e^0 + g_h^0)$ and quadratic (g_h^1) components of the exciton g factor. The results of this analysis are presented in Table I. The strong quadratic character of the hole Zeeman splitting arises from the combination of the comparatively large diameter, small height, and dilute In content in the dots investigated. First, the dot diameter ($D = 40$–50 nm) is larger than the magnetic length [$\lambda = \sqrt{\hbar/(eB)}$] over the entire range of magnetic fields of interest. Secondly, the low, almost homogeneous In concentration induces only a weak confinement potential in the core of the QDs. As a result, the quantum states that are formed in magnetic field resemble somewhat 2D Landau levels and, consequently, the HH ground states behave in a manner similar to what is known for quantum wells. Moreover, the small dot height of 6 nm (including the wetting layer) introduces a strong field-induced coupling of HH ↑ and LH ↑ states, as in narrow quantum wells.[27] The quantum-well-like dependence of the Zeeman spin splitting on magnetic field is especially pronounced for the large, In-dilute QD (iii), as illustrated in Fig. 4. The lowest-energy HH-like orbital has only a weak LH admixture (<6%) at zero magnetic field that is caused by the QD shape, In-Ga alloy profile, and inhomogeneous strain fields. This is illustrated quantitatively in the rightmost panel of Fig. 4, which shows the magnetic-field dependence of the HH-like ground states. Unlike the HH ↑, the HH ↓-like ground state effectively decouples from the LH bands as the magnetic field increases and, thus, its LH character weakens at higher fields.

TABLE I. Linear $(g_e^0 + g_h^0)$ and quadratic (g_h^1) components of the exciton g factor for QD_A, QD_B, QD_C, and QD_D presented in Figs. 2 and 3.

	$g_e^0 + g_h^0$	g_h^1 (T^{-1})
QD_A	0.58 ± 0.02	0.016 ± 0.002
QD_B	− 0.19 ± 0.03	0.028 ± 0.002
QD_C	− 0.59 ± 0.01	0.026 ± 0.001
QD_D	− 0.89 ± 0.03	0.032 ± 0.002

B. Polarization properties

The observed B-field-induced HH-LH mixing discussed in the previous section has no effect on the degree of circular polarization since a magnetic field applied along the growth direction of the QDs cannot lower the rotational symmetry of the Hamiltonian. This expectation was confirmed by the results of our calculations, which revealed a negligible and magnetic-field-independent reduction of the degree of polarization ($\approx 10^{-7}$) for magnetic fields up to $B = 15$ T. This can be clearly seen from the calculated absorption spectra for $\sigma^{\pm}$-polarized light that are presented in Fig. 5(a) for a lens-shaped model dot with a diameter of 50 nm and inverse trumpetlike In composition with $x^{\text{apex}} = 0.40$ and $x^{\text{min}} = 0.20$, chosen to represent a dot similar to QD_C or QD_D in Figs. 2 and 3. For clarity, the spectra are centered around the mean energy of the two bright exciton ground states. The spectra clearly show that the polarization of the QD levels is unaffected by the elevated external magnetic field, in accord with our expectations, as discussed in Sec. III.

The negligible loss of degree of polarization originates from terms in the Hamiltonian that lower the symmetry from C_4 to C_2 and from C_{4v} to C_{2v} with and without external magnetic fields, respectively. A strong breaking of C_4 symmetry has been observed for elongated GaAs-AlGaAs (Ref. 36) and CdTe-ZnTe (Ref. 37) quantum dots, as well as for GaAs-AlGaAs QDs, which were grown along the reduced symmetry [111] direction.[38] In contrast, in symmetrically shaped InGaAs-GaAs QDs grown on a [001] surface, the primary symmetry-breaking term stems solely from the piezoelectric field.[39] In the large, In-dilute QDs studied here, the strain field is weak with almost axial symmetry and the piezoelectric

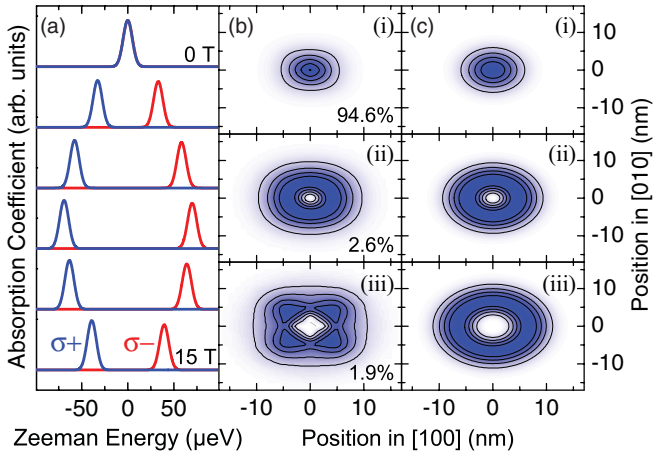

FIG. 5. (Color online) (a) Polarization-resolved ground-state absorption spectra for a QD of the type $QD_{C/D}$ as the magnetic field increases from 0 to 15 T. (b) In-plane envelope-function probability density looking along the QD growth direction of the (i) HH ↑, (ii) LH ↑, and (iii) LH ↓ component of the predominantly HH ↑ ground state for the full Hamiltonian. The numbers in the lower right corner of each panel indicate the total contribution to the wave function. (c) Constant probability density along the confinement direction for quantum-well Landau levels corresponding in the axial approximation to the components [(b) (i)–(iii)] of the full Hamiltonian.

field is negligible, especially in the center of the QD where the heavy-hole-like ground state is localized. In C_4 symmetry, the optical selection rules for circularly polarized light are strict. This has been shown in detail for hole bands of bulk Ge in the presence of uniaxial strain and magnetic fields.[40] The results are based on symmetry arguments alone and can readily be applied to QDs with the same symmetry class. Our calculations show that, even a 2:1 elongation of the QDs in the plane leads only to an extremely small reduction of the degree of polarization of the order of $\sim 10^{-3}$. This reduction is so tiny due to the large size of our QDs: The ground-state wave functions are localized in the center of the QDs, and shape anisotropy in the dot periphery has only a very weak influence on the orbital states. A more intuitive picture is obtained for full axial symmetry, which is almost realized in near perfect lens-shaped QDs (since $\gamma_2 \approx \gamma_3$). In this case, the projection of total angular momentum m_J is a good quantum number. Moreover, selection rules for $\sigma^{\pm}$ transitions are strict and become $\Delta m_J = \pm 1$. If, in addition, the magnetic length is smaller than the QD radius, the components of the QD ground states increasingly resemble combinations of Landau levels with HH/LH Bloch functions in the lateral directions.[31,40] This is realized for our QDs for magnetic fields above 5 T where the magnetic length $\lambda = \sqrt{\hbar/(eB)} \approx 11$ nm. In the presence of a magnetic field, the rotational symmetry is preserved and only states having the same total angular momentum projection are mixed.[41]

Figures 5(b) (i)–(iii) and 5(c) (i)–(iii) compare the admixture of different band spin states, namely HH ↑, LH ↑, and LH ↓, in the predominantly HH ↑-like ground-state wave function. To a very good approximation, it is composed of $(N, m_j) = (0,3/2)$, $(1,1/2)$, and $(2,-1/2)$ states, each of which combine to produce $m_J = 3/2$. The HH ↑ component $(0,3/2)$ and the LH ↑ component $(1,1/2)$, shown in Fig. 5(b) (i) and (ii), respectively, were obtained by detailed calculations and show good agreement with the corresponding Landau levels [Fig. 5(c) (i) and (ii)] in the axial approximation. The small LH ↓ component $(2,-1/2)$ [Fig. 5(b) (iii)] is affected substantially by C_4 symmetry terms in the Hamiltonian. However, it contributes only 1.9% to the total wave function and, as noted before, C_4 symmetry is enough to guarantee a high degree of polarization.

V. SUMMARY

In summary, strongly magnetic-field-dependent exciton g factors were observed in InGaAs self-assembled QDs. The microscopic origin of nonlinear Zeeman splitting was accounted for by eight-band $\mathbf{k} \cdot \mathbf{p}$ simulations using realistic parameters (size and In composition) that were directly extracted from X-STM measurements. The combined effect of dilute In composition and relatively large dot lateral size was shown to result in strong field-induced mixing of the HH-LH orbital states in high magnetic fields. This mixing manifests itself as a quadratic variation of the hole Zeeman splitting on the external magnetic field. Similar effects are negligible for the electron and have previously been observed only in thin two-dimensional systems.

ACKNOWLEDGMENTS

This work is funded by the Deutsche Forschungsgemeinschaft via Grant No. SFB-631 and the excellence cluster Nanosystems Initiative Munich and the European Union via SOLID (FP7-248629) and S3Nano (FP7-289795). G.A. also thanks the Technische Universität München Institute for Advanced Study for support.

*jovanov@wsi.tum.de

[1] R. Hanson, L. P. Kouwenhoven, J. R. Petta, S. Tarucha, and L. M. K. Vandersypen, Rev. Mod. Phys. **79**, 1217 (2007).

[2] F. H. L. Koppens, C. Buizert, K. J. Tielrooij, I. T. Vink, K. C. Nowack, T. Meunier, L. P. Kouwenhoven, and L. M. K. Vandersypen, Nature (London) **442**, 766 (2006).

[3] M. Kroner, K. M. Weiss, B. Biedermann, S. Seidl, S. Manus, A. W. Holleitner, A. Badolato, P. M. Petroff, B. D. Gerardot, R. J. Warburton, and K. Karrai, Phys. Rev. Lett. **100**, 156803 (2008).

[4] J. Pingenot, C. E. Pryor, and M. E. Flatté, Appl. Phys. Lett. **92**, 222502 (2008).

[5] T. Andlauer and P. Vogl, Phys. Rev. B **79**, 045307 (2009).

[6] J. Pingenot, C. E. Pryor, and M. E. Flatté, Phys. Rev. B **84**, 195403 (2011).

[7] G. Salis, Y. Kato, K. Ensslin, D. C. Driscoll, A. C. Gossard, and D. D. Awschalom, Nature (London) **414**, 619 (2001).

[8]M. F. Doty, M. Scheibner, I. Ponomarev, E. A. Stinaff, A. S. Bracker, V. L. Korenev, T. L. Reinecke, and D. Gammon, Phys. Rev. Lett. **97**, 197202 (2006).
[9]F. Klotz, V. Jovanov, J. Kierig, E. C. Clark, D. Rudolph, D. Heiss, M. Bichler, G. Abstreiter, M. S. Brandt, and J. J. Finley, Appl. Phys. Lett. **96**, 053113 (2010).
[10]V. Jovanov, T. Eissfeller, S. Kapfinger, E. C. Clark, F. Klotz, M. Bichler, J. G. Keizer, P. M. Koenraad, G. Abstreiter, and J. J. Finley, Phys. Rev. B **83**, 161303(R) (2011).
[11]C. E. Pryor and M. E. Flatte, Phys. Rev. Lett. **96**, 026804 (2006).
[12]J. van Bree, A. Y. Silov, P. M. Koenraad, M. E. Flatté, and C. E. Pryor, Phys. Rev. B, e-print arXiv:1111.5439 (cond-mat.mes-hall).
[13]M. J. Snelling, E. Blackwood, C. J. McDonagh, R. T. Harley, and C. T. B. Foxon, Phys. Rev. B **45**, 3922 (1992).
[14]R. J. Warburton, R. J. Nicholas, S. Sasaki, N. Miura, and K. Woodbridge, Phys. Rev. B **48**, 12323 (1993).
[15]S. Fafard, Z. R. Wasilewski, C. N. Allen, D. Picard, M. Spanner, J. P. McCaffrey, and P. G. Piva, Phys. Rev. B **59**, 15368 (1999).
[16]C. Heyn and W. Hansen, J. Cryst. Growth **251**, 140 (2003).
[17]C. Heyn and W. Hansen, J. Cryst. Growth **251**, 218 (2003).
[18]J. G. Keizer, E. Clark, M. Bichler, G. Abstreiter, J. Finley, and P. M. Koenraad, IOP Nanotechnol. **21**, 215705 (2010).
[19]D. M. Bruls, J. W. A. M. Vugs, P. M. Koenraad, H. W. M. Salemink, J. H. Wolter, M. Hopkinson, M. S. Skolnick, F. Long, and S. P. A. Gill, Appl. Phys. Lett. **81**, 1708 (2002).
[20]P. Offermans, P. M. Koenraad, J. H. Wolter, K. Pierz, M. Roy, and P. A. Maksym, Phys. Rev. B **72**, 165332 (2005).
[21]M. A. Migliorato, A. G. Cullis, M. Fearn, and J. H. Jefferson, Phys. Rev. B **65**, 115316 (2002).
[22]V. Mlinar, M. Bozkurt, J. M. Ulloa, M. Ediger, G. Bester, A. Badolato, P. M. Koenraad, R. J. Warburton, and A. Zunger, Phys. Rev. B **80**, 165425 (2009).
[23]R. Gordon, A. G. Brolo, A. McKinnon, A. Rajora, B. Leathem, and K. L. Kavanagh, Phys. Rev. Lett. **92**, 037401 (2004).
[24]B. Gayral, J. M. Gérard, B. Legrand, E. Costard, and V. Thierry-Mieg, Appl. Phys. Lett. **72**, 1421 (1998).
[25]M. H. M. van Weert, N. Akopian, F. Kelkensberg, U. Perinetti, M. P. van Kouwen, J. G. Rivas, M. T. Borgstrm, R. E. Algra, M. A. Verheijen, E. P. A. M. Bakkers, L. P. Kouwenhoven, and V. Zwiller, Small **5**, 2134 (2009).
[26]M. Dobers, K. V. Klitzing, and G. Weimann, Phys. Rev. B **38**, 5453 (1988).
[27]N. J. Traynor, R. T. Harley, and R. J. Warburton, Phys. Rev. B **51**, 7361 (1995).
[28]R. Kotlyar, T. L. Reinecke, M. Bayer, and A. Forchel, Phys. Rev. B **63**, 085310 (2001).
[29]C. R. Pidgeon and R. N. Brown, Phys. Rev. **146**, 575 (1966).
[30]H. R. Trebin, U. Rössler, and R. Ranvaud, Phys. Rev. B **20**, 686 (1979).
[31]J. M. Luttinger, Phys. Rev. **102**, 1030 (1956).
[32]I. Vurgaftman, J. R. Meyer, and L. R. Ram-Mohan, J. Appl. Phys. **89**, 5815 (2001).
[33]T. Eissfeller and P. Vogl, Phys. Rev. B **84**, 195122 (2011).
[34]O. Stier, M. Grundmann, and D. Bimberg, Phys. Rev. B **59**, 5688 (1999).
[35]$x(x,y,z) = x^{\min} + (x^{\text{apex}} - x^{\min})\exp[-\rho/\rho_0 \exp(-z/z_0)]$, with $\rho = \sqrt{x^2+y^2}$, $\rho_0 = 0.3$ nm, and $z_0 = 1.5$ nm.
[36]T. Belhadj, T. Amand, A. Kunold, C.-M. Simon, T. Kuroda, M. Abbarchi, T. Mano, K. Sakoda, S. Kunz, X. Marie, and B. Urbaszek, Appl. Phys. Lett. **97**, 051111 (2010).
[37]Y. Léger, L. Besombes, L. Maingault, and H. Mariette, Phys. Rev. B **76**, 045331 (2007).
[38]G. Sallen, B. Urbaszek, M. M. Glazov, E. L. Ivchenko, T. Kuroda, T. Mano, S. Kunz, M. Abbarchi, K. Sakoda, D. Lagarde, A. Balocchi, X. Marie, and T. Amand, Phys. Rev. Lett. **107**, 166604 (2011).
[39]M. Grundmann, O. Stier, and D. Bimberg, Phys. Rev. B **52**, 11969 (1995).
[40]K. Suzuki and J. C. Hensel, Phys. Rev. B **9**, 4184 (1974).
[41]The total angular momentum projection of the states $m_J = m_j + N$ is a combination of the Landau oscillator state (N) and the angular momentum projection m_j of the Bloch function, namely $\pm 3/2$ and $\pm 1/2$ for heavy holes and light holes, respectively. Here, we define the Landau quantum number N in accordance with Ref. 40 as $N = a^\dagger a$, with $a = \lambda(K_x - iK_y)/\sqrt{2}$ and $a^\dagger = \lambda(K_x + iK_y)/\sqrt{2}$ with the gauge covariant k operators $\mathbf{K} = \mathbf{k} + (e/\hbar)\mathbf{A}$ for the vector potential $\mathbf{A}$. With this definition, the Landau quantum number N (=0,1,2, ...) coincides with the angular momentum projection of the Landau oscillator state. Note that in contrast to bulk and QWs, there is no good second Landau quantum number due to the lack of lateral translation symmetry in the dots.